Mon. Not. R. Astron. Soc. **309**, 651–658 (1999)

Does magnetic pressure affect the intracluster medium dynamics?

D. R. Gonçalves[1,2]★ and A. C. S. Friaça[1]

[1]*Instituto Astronômico e Geofísico – USP, Av. Miguel Stefano 4200, 04301-904 São Paulo, SP, Brazil*
[2]*Instituto de Astrofísica de Canarias, E-38200 La Laguna, Tenerife, Spain*

Accepted 1999 June 15. Received 1999 June 14; in original form 1998 December 2

ABSTRACT

A possible discrepancy found between the determination of mass of the intracluster medium (ICM) from gravitational lensing data and that from X-ray observations has been much discussed in recent years. For instance, Miralda-Escudé & Babul found that the mass estimate derived from gravitational lensing can be as much as a factor of 2–2.5 larger than the mass estimate derived from analysis of the X-ray observations. Another important discrepancy related to these data is that X-ray imaging, with some spectral resolution, suggests that the mass distribution of the gravitating matter, mostly dark matter, has a central cusp, or at least that the dark matter is more centrally condensed than the X-ray-emitting gas, and also with respect to the galaxy distribution (Eyles et al.), at variance with what is expected from the most accepted models of formation of large-scale structure. Could these discrepancies be a consequence of the standard description of the ICM, in which hydrostatic equilibrium maintained by thermal pressure is assumed? In analogy to the interstellar medium of the Galaxy, a non-thermal term of pressure is expected, which contains contributions of magnetic fields, turbulence and cosmic rays. We follow the evolution of the ICM, considering a term of magnetic pressure, aiming at answering the question of whether or not these discrepancies can be explained via non-thermal terms of pressure. Our results suggest that the magnetic pressure could only affect the dynamics of the ICM on scales as small as $\lesssim 1$ kpc. Our models are constrained by the observations of large- and small-scale fields, and we are successful at reproducing available data, for both Faraday rotation limits and inverse Compton limits for the magnetic fields. In our calculations, the radius (from the cluster centre) in which magnetic pressure reaches equipartition is smaller than radii derived in previous works. The crucial difference in our models is our more realistic treatment of the magnetic field geometry, and the consideration of a sink term in the cooling flow which reduces the amplification of the field strength during the inflow. In addition, the magnetic field calculations are changed after the cooling flow has been formed.

Key words: galaxies: clusters: general – cooling flows – galaxies: magnetic fields – gravitational lensing – X-rays: galaxies.

1 INTRODUCTION

Since the work of Loeb & Mao (1994), the possibility of explaining the discrepancies in mass determinations, found by Miralda-Escudé & Babul (1995), via non-thermal pressure support has been widely discussed (see also Wu & Fang 1996, 1997; Wu et al. 1998). The discrepancy arises from the two most promising techniques for obtaining the masses of clusters of galaxies. On the one hand, the determination of masses in clusters of galaxies, via X-ray data, is based on the hypothesis that the ICM is in hydrostatic equilibrium with the gravitational potential, using the radial profiles of density and temperature. There are uncertainties in the determination of the temperature profiles, particularly for radii > 1 Mpc, and for most systems only a mean emission-weighted X-ray temperature is available (radial-temperature profiles are available for only a few clusters, e.g. Allen & Fabian 1994; Nulsen & Böhringer 1995). On the other hand, gravitational lensing measures the projected surface density of matter, a method which makes no assumptions on the dynamical state of the gravitating matter (Fort & Mellier 1994; Miralda-Escudé & Babul 1995; Smail et al. 1997).

One can find in the literature some attempts to resolve the

★ E-mail: denise@ll.iac.es (DRG); amancio@iagusp.usp.br (ACSF)

discrepancy between X-ray and gravitational lensing mass measurements of clusters of galaxies. For instance, Allen (1998) studied in detail a sample of 13 galaxy clusters (including cooling flows, intermediate and non-cooling flows systems) with the goal of comparing X-ray and lensing mass measurements. His conclusions pointed out that, at least for cooling-flow systems, which are more relaxed systems, this discrepancy is completed resolved and, therefore, non-thermal pressures can be discarded in these systems.

The magnetic field of the ICM can be obtained via Faraday rotation, owing to the effect of magnetic field on the polarized radio emission from the cluster or the background radio sources. The polarization plane of linearly polarized radiation is rotated during the passage through a magnetized plasma. The angle of rotation is $\phi = (RM)\lambda^2$, where RM is the rotation measure and λ the radiation wavelength (see Sarazin 1992 for a review). In clusters with diffuse radio emission, X-ray observations can give a lower limit to the strength of the magnetic field. Typically, this limit is $B \geqslant 0.1\,\mu$G (Rephaeli, Gruber & Rothschild 1987) on scales of ~ 1 Mpc. In the case of Faraday rotation, the information obtained is the upper limit on the intensity of the field, and the measured values are $RM \leqslant 100\,\mathrm{rad\,m^{-2}}$, which is more or less consistent with an intracluster field of $B \sim 1\,\mu$G, with a coherence length of $l_B \leqslant 10\,$kpc. This strength of the magnetic field corresponds to a ratio of magnetic pressure to gas pressure of $p_B/p_{\rm gas} \leqslant 10^{-3}$, implying that B does not influence the cluster dynamics (at least on large scales).

At inner regions of the cooling-flow clusters, the magnetic fields are expected to be amplified owing to the gas compression (Soker & Sarazin 1990). If they are frozen in the mass-flow flux, and if this flux is homogeneous and spherically symmetric, $B \propto r^{-1}$ and $RM \propto r^{-1}$ ($p_B \propto r^{-2}$ and the gas pressure increases slowly). Even in this case p_B reaches equipartition at a radius r_B of $r_B \sim 1\,\mathrm{kpc}\ (B/1\,\mu\mathrm{G})^{1/2}\ (\dot{M}/100\,\mathrm{M_\odot\,yr^{-1}})^{1/3}$. In these inner regions, many sources with very strong Faraday rotations were observed, in which the rotation measure can reach values of $RM \sim 4000\,\mathrm{rad\,m^{-2}}$ [radio sources associated with the central galaxies of the clusters with very strong cooling flows (M87/Virgo, Cyg A, Hydra A, 3C 295, A1795)], implying, $B \geqslant 10\,\mu$G at $l_B \sim 1\,$kpc (Taylor & Perley 1993; Ge & Owen 1993, 1994). These observations strongly suggest that the Faraday rotation is created by magnetic fields within the cooling-flow clusters.

Another promising method for estimating the cluster-scale magnetic field, as cited above, is the detection of cospatial inverse Compton X-ray emission with the synchrotron plasma emission (the 3-K background photons scattering off the relativistic electrons can produce a diffuse X-ray emission) (Rephaeli & Gruber 1988). Therefore, this method provides limits on the cluster-scale magnetic fields, in addition to limits on the non-thermal amount of X-ray emission (or even on the relativistic electron energy) in galaxy clusters. This type of detection of cluster magnetic fields, using *ROSAT* PSPC data and also the 327-MHz radio map of Abell 85 (a cooling-flow cluster, with a central dominant cD galaxy and about $100\,\mathrm{M_\odot\,yr^{-1}}$), leads to an estimate of $(0.95 \pm 0.10)\,\mu$G (Bagchi, Pislar & Lima Neto 1998). However, even non-cooling-flow clusters present this diffuse, relic radio source, which can be used to estimate magnetic field strength. For instance, Ensslin & Biermann (1998) studied limits on the Coma cluster magnetic field strength, using these multifrequency observations. They showed that the central-magnetic-field limit is $B > 0.3\,\mu$G. Others have determined the strength of the magnetic field for the Coma cluster, using different techniques and obtaining similar values: $B \leqslant 1.2\,\mu$G (Lieu et al. 1996); $B > 0.4\,\mu$G (Sreekumar et al. 1996). For the same cluster (Coma), but using the Faraday rotation measure, Feretti et al. (1995) estimated magnetic fields of $6.0\,\mu$G (at scales of 1 kpc), and Kim et al. (1990) estimated $1.7\,\mu$G (at scales of 10 kpc).

The above scenarios allow us to conclude that for both methods the observational resolution of the telescope limits the detection of smaller-scale magnetic fields, implying that at scales smaller than 1 kpc the magnetic field strength can be higher (Ensslin et al. 1997). Another point to be noted is that the Faraday rotation measure always gives values higher than inverse Compton/CBM measures. Anyway, these fields are present in the ICM and therefore justify the kind of study we present here. Other theoretical works concerning the magnetic pressure on the ICM are available (for instance Soker & Sarazin 1990; Tribble 1993; Zoabi, Soker & Reveg 1996) and we briefly compare our results with those obtained by these authors.

Our goal of this paper is to attempt to answer the question of whether or not magnetic support can be relevant in cooling-flow clusters, using a more realistic treatment of the magnetic-field geometric evolution. The scope of the paper is as follows: in Section 2 we present the hydrodynamical equations and the method applied for their solution; Section 3 describes our models and results compared with the available observations; and in Section 4 we discuss our results in the light of others obtained in previous works, as well our main conclusions.

2 EVOLUTION OF THE ICM WITH MAGNETIC PRESSURE

The evolution of the intracluster gas is obtained by solving the hydrodynamic equations of mass, momentum and energy conservation:

$$\frac{\partial \rho}{\partial t} + \frac{1}{r^2}\frac{\partial}{\partial r}(r^2 \rho u) = -\omega\rho \tag{1}$$

$$\frac{\partial u}{\partial t} + u\frac{\partial u}{\partial r} = -\frac{1}{\rho}\frac{\partial p_{\rm t}}{\partial r} - \frac{GM(r)}{r^2} \tag{2}$$

$$\frac{\partial U}{\partial t} + u\frac{\partial U}{\partial r} = \frac{p_{\rm t}}{\rho^2}\left(\frac{\partial \rho}{\partial t} + u\frac{\partial \rho}{\partial r}\right) - \Lambda\rho, \tag{3}$$

where u, ρ, $p_{\rm t}$, U are the gas velocity, density, total pressure and the specific internal energy. The equation of state relates U and the temperature T,

$$U = \frac{3}{2}\frac{k_{\rm B}T}{\mu m_{\rm H}} \tag{4}$$

($k_{\rm B}$ is Boltzmann's constant, $m_{\rm H}$ is the hydrogen atom mass and $\mu = 0.62$ is the mean molecular weight of a fully ionized gas with 10 per cent helium by number). The mass distribution, $M(r)$, is the result of the contribution of the X-ray-emitting gas plus the cluster collisionless matter (which is the sum of the contributions of galaxies and dark matter – the latter being dominant), i.e. $M(r) = M_{\rm g}(r) + M_{\rm cl}(r)$. $M_{\rm cl}(r)$ follows

$$\rho_{\rm cl}(r) = \rho_0\left(1 + \frac{r^2}{a^2}\right)^{-3/2}, \tag{5}$$

in which ρ_0 and a (the cluster core radius) are related to σ (the line-of-sight velocity dispersion) via: $9\sigma^2 = 4\pi G a^2 \rho_0$.

The total pressure $p_{\rm t}$ is the sum of thermal and magnetic

pressure, e.g. $p_t = p + p_B$. The constraints to the magnetic pressure come from observations, from which $p_B = B^2/8\pi \simeq 4 \times 10^{-14}\,\mathrm{erg\,cm^{-3}\,s^{-1}}$ (cf. Bagchi et al. 1998) for a diffuse field located at $\sim 700\,h_{50}^{-1}$ kpc from the cluster centre. Throughout this paper we will mainly use the ratio between magnetic and thermal pressures, or the β-parameter, $\beta = p_B/p$.

The sink term $\omega\rho$ in the mass equation describes the removal of mass from the gas flow by thermal instabilities. The importance of the gas removal was studied in detail by Friaça (1993) following the q-description described by White & Sarazin (1987). The sink is particularly important when one searches for a steady-state solution of the cooling flow without an implausibly large accumulation of mass at the centre. In fact, the condensations formed by the sink will probably give rise to stars, planetary bodies or cold dense clouds which in turn will constitute a halo surrounding the central dominant galaxy. We assume isobaric removal, so that the sink does not introduce any additional term in the energy equation. Summing up the physics contained in this term one can say that the specific mass removal rate is $\omega = q/t_c$, where the denominator is the instantaneous isobaric cooling time, such that the removal efficiency q relates the cooling time to the growth time-scale of the thermal instability in the cooling flow. We assume q to be between 1.0 and 1.5, which are the q-values found to be more consistent with the observations (Friaça 1993).

The cooling function adopted, $\Lambda(T)$, is the cooling rate per unit volume. Because there is no ionization equilibrium for temperatures lower than 10^6 K, we adopt a non-equilibrium cooling function for the gas at $T < 10^6$ K (the recombination time of important ions is longer than the cooling time at these temperatures). The cooling function was calculated with the atomic data base of the photoionization code AANGABA (Gruenwald & Viegas 1992). The adopted abundances are subsolar as appropriate for the ICM (Edge & Stewart 1991; Fabian 1994; Grevesse & Anders 1989).

Despite the presence of steep temperature gradients, we did not consider thermal conduction in our models. This can be justified by the fact that on a global scale, cooling-flow clusters contain cooler gas near the centre and hotter gas further out. Therefore, the presence of cooling flows is itself a proof that the thermal-conduction effect is, at least, reduced in the ICM. Models show that thermal conduction would erase the observed density and temperature gradients in cooling flows, unless it is inhibited (see, for instance, Friaça 1986; David & Bregman 1989). It is well known that even weak magnetic fields, if it is tangled, can inhibit the thermal conduction perpendicular to the field lines. More recently it has been argued that electromagnetic instabilities driven by temperature gradients (or electric currents in other situations) can also cause this inhibition in cooling flows (Pistinner, Levinson & Eichler 1996), even for non-tangled field lines.

A spherically symmetric Eulerian code is employed for the calculations, which are solved via the finite-difference scheme based on Cloutman (1980). The grid points are spaced logarithmically, with a grid of 100 cells, with the first being 50-pc wide. The innermost cell edge is located at 100 pc and the outer boundary at twice the tidal radius of the cluster. The artificial viscosity for the treatment of the shocks follows the formulation of Tscharnuter & Winkler (1979) based on the Navier–Stokes equation. The outer-boundary conditions on pressure and density are derived by including an outer fictitious cell, the density and pressure in which are obtained from extrapolation of power laws over the radius fitted to the five outermost real cells. The inner-boundary conditions are adjusted according to whether inflow (velocity at the inner boundary is extrapolated from the velocities at the innermost cell edges) or outflow (velocity is set zero) prevails locally. The initial conditions for the gas are an isothermal atmosphere ($T_0 = 10^7$ K) with 30 per cent solar abundances and density distribution following that of the cluster dark matter. The evolution is followed until the age of 14 Gyr.

The initial β value used here was derived from the magnetic field observations (using, for instance, Bagchi et al. 1998; Ge & Owen 1993, 1994; Ensslin & Biermann 1998; Ryu & Biermann 1998). We assume: frozen-in field; spherical symmetry for the flow and the cluster itself; and that at $r > r_c$ (the cooling radius, see below), the magnetic field is isotropic, i.e.

$$B_r^2 = B_t^2/2 = B^2/3,$$

and $l_r = l_t \equiv l$ (where B_r and B_t are the radial and transversal components of the magnetic field B, and l_r and l_t are the coherence length of the large-scale field in the radial and transverse directions). In order to calculate B_r and B_t for $r < r_c$ we modified the calculation of the magnetic field of Soker & Sarazin (1990) by considering an inhomogeneous cooling flow (i.e. $\dot{M}_i \neq \dot{M}$ varies with r). Therefore, the two components of the field are then given by

$$\frac{\mathrm{D}}{\mathrm{D}t}(B_r^2 r^4 \dot{M}^{-2}) = 0$$

and

$$\frac{\mathrm{D}}{\mathrm{D}t}(B_t^2 r^2 u^2 \dot{M}^{-1}) = 0.$$

In our models we take the cooling radius r_c as the reference radius. In fact, we modify the geometry of the field when and where the cooling time becomes less than 10^{10} yr (usually adopted as the condition for the development of a cooling flow). Therefore, our condition to assume a non-isotropic field is $t_{coo} \equiv 3k_BT/2\mu m_H \Lambda(T)\rho \leqslant 10^{10}$ yr. After the formation of the cooling flow, in the inner regions of the ICM, the magnetic field geometry is changed, following the enhancement of the radial component of the field, owing to the enhancement of the density.

3 MODELS AND RESULTS

In this section we present the results of our models. There are four parameters to consider in each of the models: σ, the cluster velocity dispersion; ρ_0, the initial average mass density of the gas; a, the cluster core radius; and β_0, the initial magnetic pressure to thermal pressure ratio. We adopted the removal efficiency $q = 1.5$.

The most important results of our models are shown in the Figs. that we describe below, for which we assume: $\sigma = 1000\,\mathrm{km\,s^{-1}}$ and $a = 250$ kpc. First of all, the evolution we follow here is characteristic of cooling-flow clusters and in this scenario we discuss the evolution of the basic thermodynamic parameters. Considering the overall characteristics of our models, we will compare the results with the very recent study based on *ROSAT* observations of the cores of clusters of galaxies, by Peres et al. (1998), focusing on cooling flows in an X-ray flux-limited sample (containing the brightest 55 clusters over the sky in the 2–10 keV band). Comparing the present models with Peres et al.'s (1998) deprojection results, we see that the central cooling time adopted here as our cooling-flow criterion, e.g. $t_{coo} \lesssim 10^{10}$ yr, is typical for

a fraction of between 70 and 90 per cent of their sample. They also discuss briefly the cooling-flow age, remembering that in hierarchical scenarios for the formation of structures in the Universe, clusters are formed from smaller substructures by mergers, and therefore the estimation of the cooling-flow ages (and the cluster ages themselves) is complicated. Anyway, they determine the fraction of cooling-flow clusters in their sample considering a factor of 2 in the ages and conclude that the fraction does not vary that much (from 13 to 6 Gyr, the fraction varies from 70 to 65 per cent). This allows us to conclude that our models, in which cooling flows arise between the cluster ages of $\sim$ 7–9 Gyr, are typical for their sample. As a matter of fact, the time at which the cooling-flow structure is formed depends strongly on the initial density that we adopted. For models with $\rho_0 = 1.25 \times 10^{-28}\,\mathrm{g\,cm^{-3}}$ it is formed at $\sim$ 9 Gyr, while for the models with $\rho_0 = 1.5 \times 10^{-28}\,\mathrm{g\,cm^{-3}}$ the cooling-flow structure is formed at $\sim$ 7 Gyr. We will come back to this point later when analysing the field anisotropy.

The characteristics of our models are summarized using four typical sets of initial parameters, and some details are discussed that arose from a study of a larger grid of parameters. Therefore, each model is characterized by its position in the (ρ_0,β_0) parameter space: model I ($\rho_0 = 1.5 \times 10^{-28}\,\mathrm{g\,cm^{-3}}, \beta_0 = 10^{-2}$); model II ($\rho_0 = 1.5 \times 10^{-28}\,\mathrm{g\,cm^{-3}}, \beta_0 = 10^{-3}$); model III ($\rho_0 = 1.25 \times 10^{-28}\,\mathrm{g\,cm^{-3}}, \beta_0 = 10^{-2}$); and model IV ($\rho_0 = 1.25 \times 10^{-28}\,\mathrm{g\,cm^{-3}}, \beta_0 = 10^{-3}$).

Fig. 1 shows the evolution of density and temperature profiles corresponding to model I, from which the presence of the cooling flow on later stages of the ICM evolution and at inner regions is remarkable if one notices the steep gradients of these quantities. In order to better understand how the magnetic field geometry is modified after the cooling-flow formation, e.g. after the steepness on the temperature and density gradients, we follow the evolution of the degree of anisotropy, using the concepts previously defined in Section 2, concerning the geometry of the magnetic field. Hereafter, we call the 'degree of anisotropy' the ratio $B_\mathrm{t}/B_\mathrm{r}$, noting that for the isotropic case it is $\sqrt{2}$, and the more anisotropic the field geometry is, the smaller the ratio is. Therefore, we present in Fig. 2 the evolution of the degree of anisotropy since $\sim$ 3.3 Gyr, comparing models I and III, in which one can see, clearly, that the anisotropy begins decreasing at earlier times for models with higher ρ_0 (model I) than for models with lower values of ρ_0 (model III). From Fig. 2 we can conclude that the degree of anisotropy can be seen as a sensor of the presence of the cooling flow. In other words, the change in the degree of anisotropy can be used as another criterion to indicate the epoch, in the ICM evolution, in which the cooling flow appears.

These results can also be discussed in the light of some observational works in which the limits to the magnetic field strength on large and small scales of the cooling flow clusters are given. Following this kind of observation, as previously seen in the Introduction, we choose two values of magnetic field strength derived by the authors below. The first one is presented in Bagchi et al. (1998) who estimated, from inverse Compton X-ray emission with the synchrotron emission plasma, a cluster-scale (700 kpc) magnetic field strength of $(0.95 \pm 0.10)\,\mu$G for Abell 85 (a cooling-flow cluster with a central dominant cD galaxy and $\dot{M} \simeq 100\,\mathrm{M_\odot\,yr^{-1}}$). The second one is presented in two papers of Ge & Owen (1993, 1994), in which they present and discuss rotation measures and the related intensity of the magnetic field, giving a range of this intensity at scales of 10 kpc. Our results for the magnetic field strength and also for pressures, on large and small scales, are compared with the chosen observed ones, in Figs 3 and 4. Remembering that the time at which the cooling flow arises is closely related to ρ_0, one can expect distinct results on the evolution of the field intensity from, for instance, model I to model III. However, this evolution can be better explained by comparing model I (Fig. 3) with model II (Fig. 4), because these two models have the same initial density but distinct β_0.

Our best model, in terms of the magnetic field strength compared with observations, is model I ($\rho_0 = 1.5\times 10^{-28}\,\mathrm{g\,cm^{-3}}$, $\beta_0 = 10^{-2}$). From Fig. 3 it is possible to see that on scales of 700 kpc the magnetic field expected for the model is higher than the observed one (considering, of course, the profile corresponding to redshift zero, or evolution times on the order of 13–14 Gyr), while on scales of 10 kpc the model gives a value lower than the observed one. Meanwhile, at least on scales of 700 kpc, the situation is inverted if one takes a look on Fig. 4, for which $\rho_0 = 1.5 \times 10^{-28}\,\mathrm{g\,cm^{-3}}$, but $\beta_0 = 10^{-3}$. Given the uncertainties of the observations, we can say that our models are in agreement with the magnetic field estimations available.

In Figs. 5 and 6 we show the evolution of the magnetic and thermal pressures, or in other words, β-evolution, for models I and II, respectively, at later times of the ICM evolution, in order to analyse when and where magnetic pressure reaches equipartition.

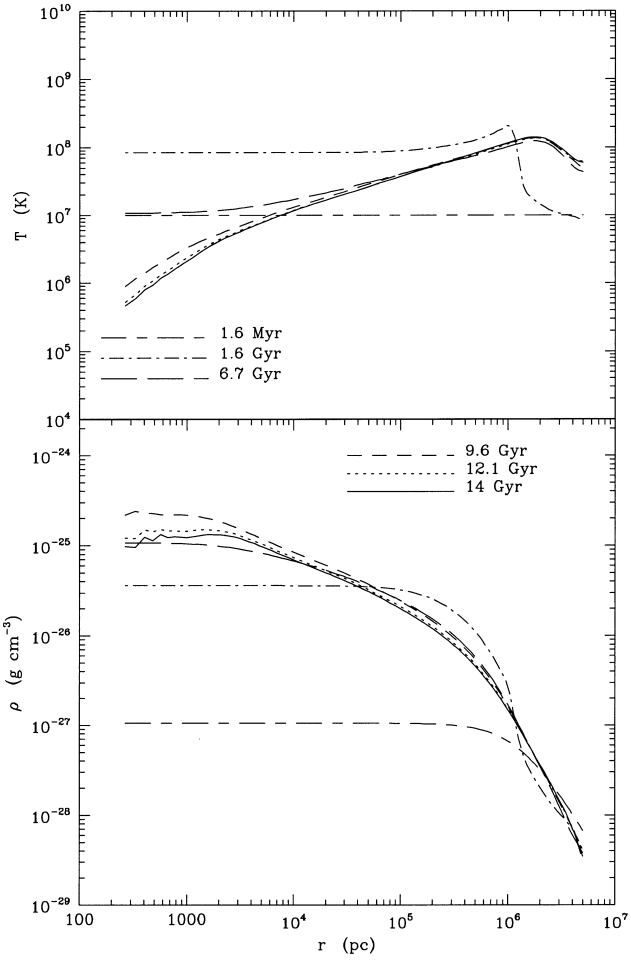

Figure 1. Evolution of the density and temperature profiles. The curves represent early and late stages of the ICM evolution, as labelled, for model I. Notice the steep gradients of these quantities, i.e. the presence of the cooling flow, at inner regions of the cluster, at later stages of the ICM evolution.

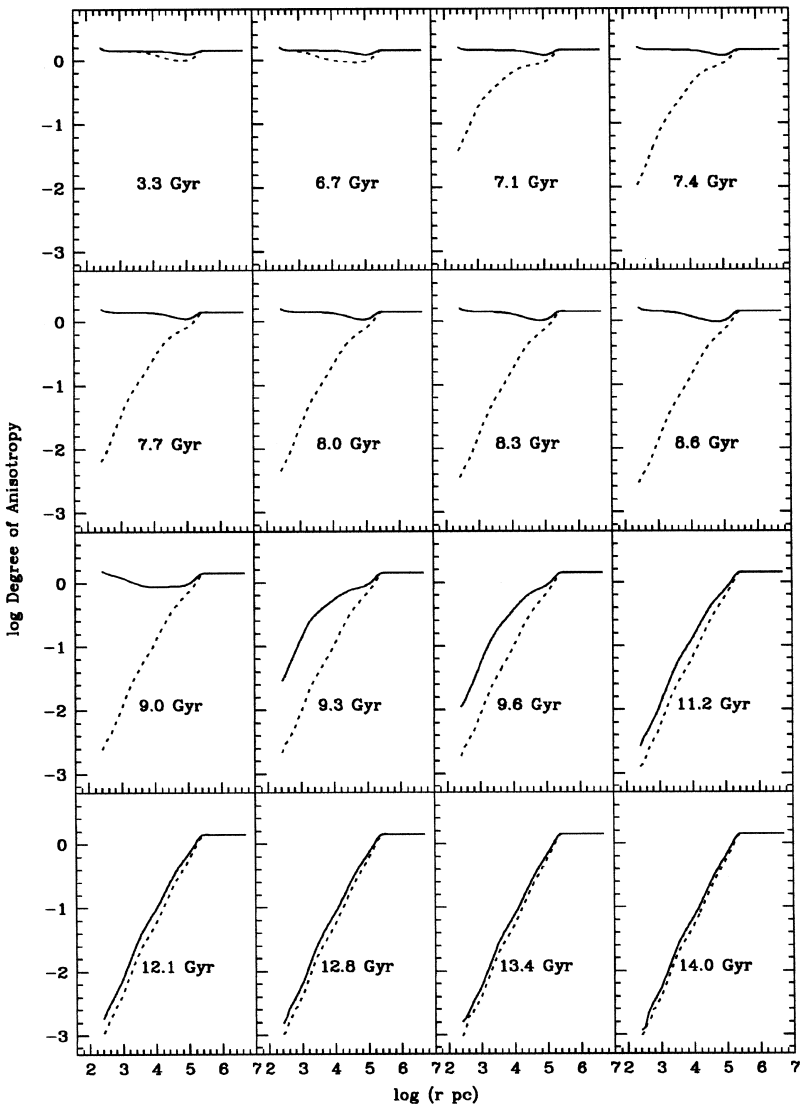

Figure 2. Evolution of the anisotropy degree, ratio of the tangential to radial magnetic field components, for model I (dashed lines) and III (full lines), at late stages of the ICM evolution. Notice that the presence of the cooling flow, at inner regions, $\lesssim 200$ kpc, and at late stages, $\gtrsim 9.6$ Gyr, of the ICM evolution (see Fig. 1) matches very well with the decrease of the anisotropy degree, and that it occurs earlier for model I.

Obviously the magnetic pressure is compatible with the magnetic field intensities and may be compared with the values determined by, for instance, Bagchi et al. (1998), $p_B = B^2/8\pi \simeq 4 \times 10^{-14}\,\mathrm{erg\,cm^{-3}\,s^{-1}}$, at scales of 700 kpc, on the present time. From the analysis of the magnetic pressures expected from our models it is clear that they agree, as well as the magnetic field strength, with the observations. Here again model I appears to be the best one, with $\beta_0 = 10^{-2}$, but the values obtained from model II are also not far from the observed ones. Noting also that magnetic pressure and/or magnetic intensity do not change very much after 12 Gyr, for both cases. Results presented in Figs 3–6 indicate that we should adopt an intermediate initial value for β (like $\beta_0 = 5 \times 10^{-3}$) in order to obtain a magnetic field intensity in better agreement with the observations, at least on scales of 700 kpc. Nevertheless, such an exercise would not solve the match of models and observations on smaller scales, because $\beta_0 \simeq 5 \times 10^{-3}$ would decrease the magnetic pressure on scales of 10 kpc, at the present time, as a result of the present modelling assumptions (see Fig. 4).

Other proposals for the amplification of the magnetic field in the centre of the cooling-flow clusters are: (i) rotation-driven mechanisms, in which the twisting of the magnetic flux tubes and/or the operation of fast $\alpha - \omega$ dynamo are responsible for the increase of the magnetic strength (Godon, Soker & White 1998); (ii) turbulence-induced amplification (Eilek 1990; Mathews & Brighenti 1997). However, these processes cannot account for the strong magnetic fields observed in the central regions, confirming the expectations previously discussed by authors like Goldshmidt & Rephaeli (1993) and Carvalho (1994).

4 DISCUSSION AND CONCLUSIONS

The present models are in many aspects similar to the one of Soker & Sarazin (1990). However, there are two important differences between our model and theirs: (i) they take into account only small-scale magnetic field effects; and (ii) they consider homogeneous cooling flow. As we consider inhomogeneous

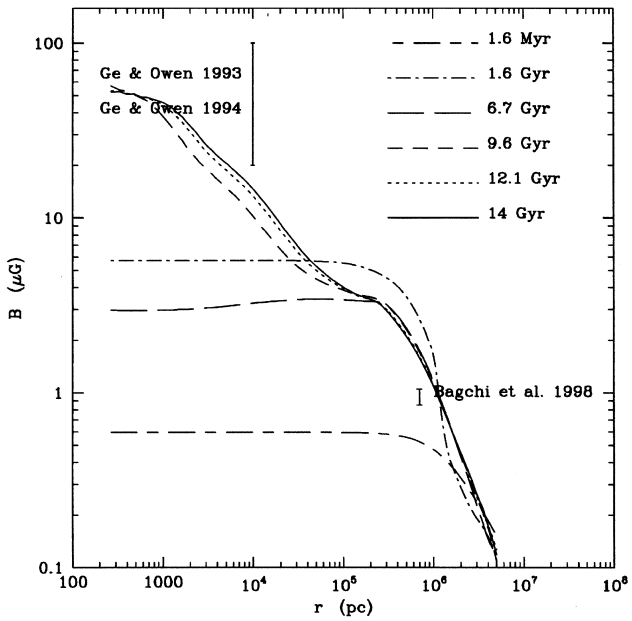

Figure 3. Evolution of the magnetic strength profiles compared with the observations. The curves represent early and late stages of the ICM evolution, as labelled, for model I ($\rho_0 = 1.5 \times 10^{-28}\,\mathrm{g\,cm^{-3}}$; $\beta_0 = 10^{-2}$). Note that the intensity B of the magnetic field at 6.7 Gyr is smaller than at 1.6 Gyr, owing to the fact that at 6.7 Gyr the ICM is on the verge of developing a cooling flow, as we can see from the drop in temperature in the central region, as shown in Fig. 1. In the evolution of the ICM before the onset of the cooling flow, the magnetic pressure keeps track of the thermal pressure, following the initial conditions for $p_B/p = \beta_0 < 1$, and the reduction in the thermal pressure just after the onset of the cooling flow is reflected in the evolution of B. Only after the cooling flow has been established, leading to amplification of B, will the intensity of the magnetic field rise to high values.

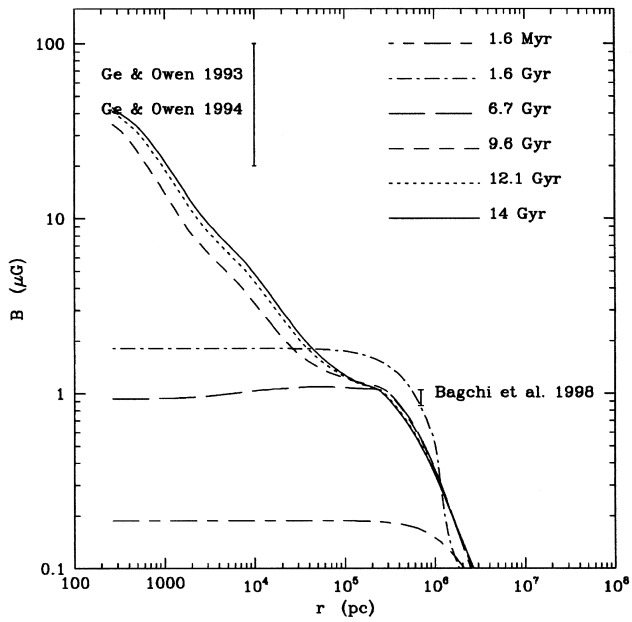

Figure 4. Evolution of the magnetic strength profiles compared with observations. The curves represent early and late stages of the ICM evolution, as labelled, for model II ($\rho_0 = 1.5 \times 10^{-28}\,\mathrm{g\,cm^{-3}}$; $\beta_0 = 10^{-3}$). See the comments on the evolution of B made in the caption of Fig. 3.

cooling flow (i.e. $\dot{M}$ decreases with decreasing r) the amplification of B is smaller in our models. As a matter of fact the magnetic pressure reaches equipartition only at a radius as small as $\gtrsim 1$ kpc (model I) or $\gtrsim 0.5$ kpc (model II), because the central increase of the β ratio is moderate in our model. Our more realistic description of the field geometry is crucial. This implies that the effect of the magnetic pressure on the total pressure of the intracluster medium, even on regions with a radius as small as a few kpc, is small. Tribble (1993), studying the formation of radio haloes in cooling-flow clusters from the point of view of the cluster evolution via mergers, suggested typical magnetic field strengths of $\sim 1\,\mu$G. In addition, Zoabi et al. (1996), studying a completely different characteristic of the ICM (magnetic fields on the support of X-ray clumps and filaments), adopted the usually assumed magnetic to pressure ratio, at small scales of 10–20 kpc, of 0.1, and following a simple geometry of the field in which it is amplified by the radial inflow, this ratio became ~ 1 at ~ 5 kpc. Again our results are more or less compatible with the ones above (for the cluster scale magnetic field), but the equipartition condition is reached at smaller scales.

There are a number of papers discussing heating processes in the inner part of the cooling-flow clusters, in particular mechanisms to power the emission lines of optical filaments, which use the magnetic energy transformed in optical emission via magnetic reconnection (Jafelice & Friaça 1996) or dissipation of Alfvén waves (Friaça et al. 1997). These works are based in the enhancement of the magnetic pressure on scales smaller than ~ 10 kpc, where the filaments are observed (Heckman et al. 1989). Finally, our results suggest that the effect of the magnetic fields on the ICM dynamics can be relevant only on very small scales: $\beta \sim 10^{-1}$, $r \lesssim 10$ kpc, and $\beta \sim 1$, $r \lesssim 1$ kpc, depending on the model adopted (see Fig. 7). From Fig. 7 one can see quite clearly that the equipartition condition is reached at smaller radii for models in which β_0 is equal to 10^{-3} (model II and model IV), emphasizing the agreement between our models, other theoretical models, and observations.

It is also quite relevant to notice that the general agreement of our models and the available data can be emphasized by the fact that observations give us only limits on the magnetic field intensities. In the case of rotation measures the limit is the upper one, in contrast with the data coming from inverse Compton scattering which give the lower limit of this quantity. Therefore, from our best model (model I, see Fig. 3) the expected field intensity is lower than the observed value (provided via rotation measures), on scales of 10 kpc, and higher than the field intensity derived from X-ray inverse Compton scattering, on larger scales (700 kpc).

That the discrepancy found in the determination of mass from gravitational lensing and from X-ray observations (Loeb & Mao 1994; Loewenstein 1994; Miralda-Escudé & Babul 1995), and in the mass distribution of the gravitating matter, mostly dark matter (Eyles et al. 1991), can be a consequence of the standard description of the ICM, in which hydrostatic equilibrium driven by thermal pressure is assumed (Fabian 1994), is a subject of discussion. Allen (1998) argued that, at least for cooling-flow clusters, the above discrepancy is resolved and, therefore, the effect of non-thermal pressures on the hydrostatic equilibrium of these systems could be completed discarded. However, it is important to point out that the radius in which magnetic pressure reaches equipartition is much smaller than the core or arc radii obtained by Allen in his analysis (~ 50 kpc, on average), implying that, despite Allen's results, at smaller scales the non-thermal pressures can be important.

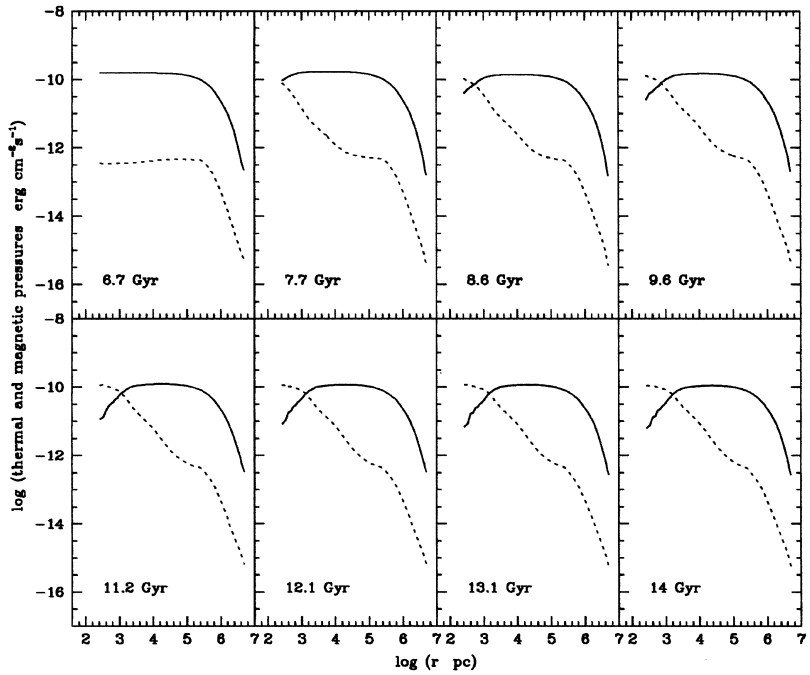

Figure 5. Evolution of the magnetic (dashed lines) and thermal (full lines) pressure profiles at late stages of the ICM evolution for model I. Notice that the magnetic pressure increases until it reaches equipartition at inner regions of the cooling flow (at scales $\lesssim 1$ kpc).

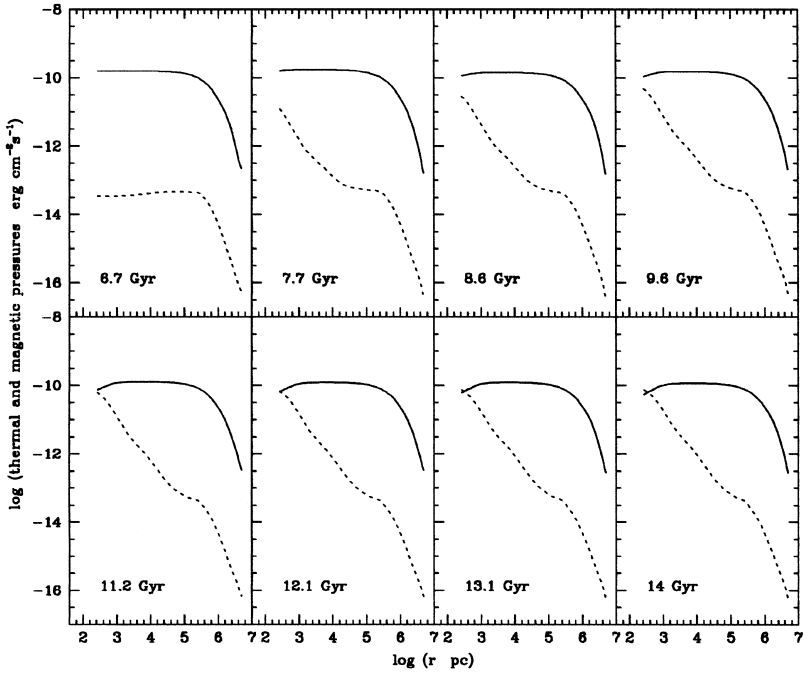

Figure 6. Evolution of the magnetic (dashed lines) and thermal (full lines) pressure profiles at late stages of the ICM evolution for model II. Notice that the magnetic pressure increases until it reaches equipartition at inner regions of the cooling flow (at scales $\lesssim 0.5$ kpc).

Theoretical models, like the one presented here, point out that magnetic pressure does affect the hydrostatic equilibrium of the ICM, but only in the inner radius, as small as ~ 1 kpc. In addition, it is important to remember that there are other sources of non-thermal pressures that could be considered jointly with the magnetic pressure before closing the discussion on whether or not non-thermal pressures can explain the discrepancies in the mass estimations of the galaxy clusters.

ACKNOWLEDGMENTS

DRG would like to thank the Brazilian agency FAPESP

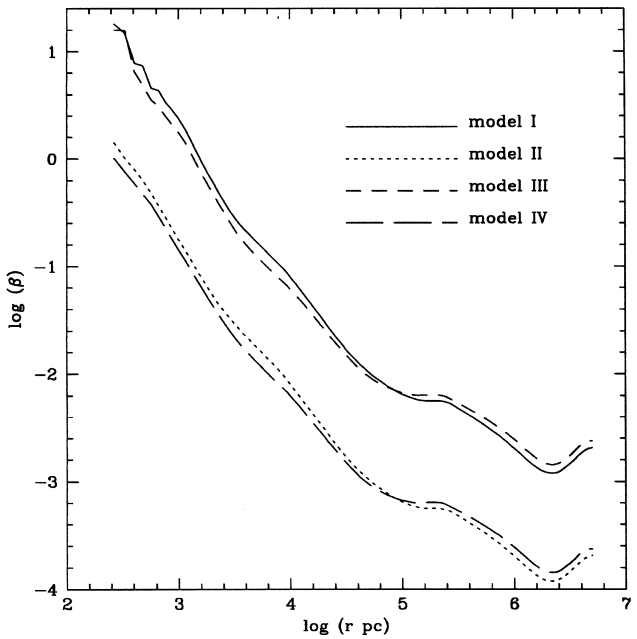

Figure 7. β profiles at 14 Gyr for models I-IV. The profiles are all quite similar, except for the fact that models with $\beta_0 = 10^{-3}$ have lower final β-values. From the Fig. it is also clear that the equipartition condition occurs at outer radii for higher β_0 models, and that anyway this condition is reached only on radii smaller than $\sim$ 1 kpc.

(97/05246-3) for its support, and ACSF would like to thank the Brazilian agency CNPq for its partial support. We would also like to acknowledge partial support from Pronex/FINEP (41.96.0908.00).

REFERENCES

Allen S. W., 1998, MNRAS, 296, 392
Allen S. W., Fabian A. C., 1994, MNRAS, 269, 409
Bagchi J., Pislar V., 1998, MNRAS, 296, L23
Carvalho J. C., 1994, A&A, 281, 641
Cloutman L. D., 1980, Los Alamos Report, LA-8452-MS
David L. P., Bregman J. N., 1989, ApJ, 337, 97
Edge A. C., Stewart A. C., 1991, MNRAS, 252, 414
Eilek J., , in, Fitchett M. J., Oergerle W. R., Danly L., 1990, Clusters of Galaxies, STScl, Baltimore, , p., 59
Ensslin T. A., Biermann P. L., 1998, A&A, 330, 90
Ensslin T. A., Biermann P. L., Kronberg P. P., Wu X.-P., 1997, ApJ, 477, 560
Eyles C. J., Watt M. P., Bertram D., Church M. J, Penman T. J., Skinner G. K., Willlmore A. P, 1991, ApJ, 376, 23
Fabian A. C., 1994, ARA&A, 32, 277
Feretti L., Dallascasa D., Giovannini G., Taglianai A., 1995, A&A, 302, 680
Fort B., Mellier Y., 1994, A&AR, 5, 239
Friaça A. C. S., 1986, A&A, 164, 6
Friaça A. C. S., 1993, A&A, 269, 145
Friaça A. C. S., Gonçalves D. R., Jafelice L. C., Jatenco-Pereira V., Opher R., 1997, A&A, 324, 449
Ge J. P., Owen F. N., 1993, AJ, 105, 778
Ge J. P., Owen F. N., 1994, AJ, 108, 1523
Godon P., Soker N., White R. E.,III 1998, AJ, 116, 37
Goldshmidt O., Rephaeli Y., 1993, ApJ, 411, 518
Grevesse N., Anders E., , in, Waddington C. J., 1989, Cosmic Abundances of Matter, AIP, New York, , p., 183
Gruenwald R. B., Viegas S. M., 1992, ApJS, 78, 153
Heckman T. M., Baum S. A., Van Breugel W. J. M., McCarthy P., 1989, ApJ, 338, 48
Jafelice L. C., Friaça A. C. S., 1996, MNRAS, 280, 438
Kim J. P., Butcher J. A., Stewart G. C., Tanaka Y., 1990, ApJ, 335, 29
Lieu R., Mittaz J. P. D., Bowyer S., Breem J. O., Lockmann F. J., Murphy E. M., Hwang C.-Y, 1996, Sci., 274, 1335
Loeb A., Mao S., 1994, ApJ, 435, L109
Loewenstein M., 1994, ApJ, 431, 91
Mathews W. G., Brighenti F., 1997, ApJ, 488, 595
Miralda-Escudé J., Babul A., 1995, ApJ, 449, 18
Nulsen P. E. J., Böhringer H., 1995, MNRAS, 274, 1093
Peres C. B., Fabian A. C., Edge A. C., Allen S. W., Johnstone R. M., White D. A., 1998, MNRAS, 298, 416
Pistinner S., Levinson A., Eichler D., 1996, ApJ, 467, 162
Rephaeli Y., Gruber D. E., 1988, ApJ, 333, 133
Rephaeli Y., Gruber D. E., Rothschild R. E., 1987, ApJ, 320, 139
Ryu D., Biermann P. L., 1998, A&A, 335, 19
Smail I., Ellis R. E., Dressler A., Couch W. J., Oemler A., Sharples R. M., Bucther H., 1997, ApJ, 479, 70
Sarazin C. L., 1992, in Fabian A. C., ed., Clusters and Superclusters of Galaxies. NATO ASI Series, p. 131
Soker N., Sarazin C. L., 1990, ApJ, 348, 73
Sreekumar P. et al., ApJ, 1996, 464, 628
Taylor G. B., Perley R. A., 1993, ApJ, 416, 554
Tribble P. C., 1993, MNRAS, 263, 31
Tscharnuter W. M., Winkler K. H., 1979, Comp. Phys. Comm., 18, 171
White R. E.,III Sarazin C. L., 1987, ApJ, 318, 612
Wu X. P., Fang L. Z., 1996, ApJ, 467, L45
Wu X. P., Fang L. Z., 1997, ApJ, 483, 62
Wu X. P., Chieuh T., Fang L. Z., Xue Y. J., 1998, MNRAS, 301, 861
Zoabi E., Soker N., Reveg O., 1996, ApJ, 460, 244

This paper has been typeset from a TEX/LATEX file prepared by the author.